ACS SENSORS

pubs.acs.org/acssensors

Article

Organelle-Level Labile Zn^{2+} Mapping Based on Targetable Fluorescent Sensors

Rong Liu, Toshiyuki Kowada, Yuyin Du, Yuta Amagai, Toshitaka Matsui, Kenji Inaba, and Shin Mizukami*

Cite This: *ACS Sens.* 2022, 7, 748–757

Read Online

ACCESS | Metrics & More | Article Recommendations | Supporting Information

ABSTRACT: Although many Zn^{2+} fluorescent probes have been developed, there remains a lack of consensus on the labile Zn^{2+} concentrations ($[Zn^{2+}]$) in several cellular compartments, as the fluorescence properties and zinc affinity of the fluorescent probes are greatly affected by the pH and redox environments specific to organelles. In this study, we developed two turn-on-type Zn^{2+} fluorescent probes, namely, ZnDA-2H and ZnDA-3H, with low pH sensitivity and suitable affinity (K_d = 5.0 and 0.16 nM) for detecting physiological labile Zn^{2+} in various cellular compartments, such as the cytosol, nucleus, ER, and mitochondria. Due to their sufficient membrane permeability, both probes were precisely localized to the target organelles in HeLa cells using HaloTag labeling technology. Using an *in situ* standard quantification method, we identified the $[Zn^{2+}]$ in the tested organelles, resulting in the subcellular $[Zn^{2+}]$ distribution as $[Zn^{2+}]_{ER} < [Zn^{2+}]_{mito} < [Zn^{2+}]_{cyto} \sim [Zn^{2+}]_{nuc}$.

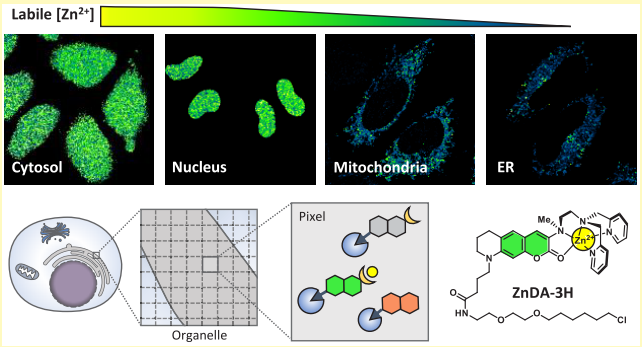

KEYWORDS: *subcellular mapping, quantification, small-molecule protein hybrid probe, organelle, labile Zn^{2+}*

Zn^{2+} is generally considered to play three main physiological roles in living cells, namely, an enzyme cofactor, a protein structural modulator, and a signaling mediator.[1] The total concentration of intracellular Zn^{2+} is estimated to be at the micromolar level, and the majority of Zn^{2+} is considered to be bound with zinc buffers such as metallothioneins and metalloproteins.[2] In addition, there exists trace amounts of labile Zn^{2+}, which is loosely bound to proteins or other biomolecules and is readily accessible by chelators, such as *N*,*N*,*N*′,*N*′-tetrakis(2-pyridylmethyl)-ethylenediamine (TPEN).[3] The strict compartmentalization and homeostasis of Zn^{2+} by zinc buffers and transporters imply the possibility of various physiological roles of Zn^{2+} at the organelle level. The transporters of zinc, namely, ZIPs (Zrt- and Irt-related proteins, SLC39s) and ZnTs (zinc transporters, SLC30s), regulate the concentration of Zn^{2+} in each organelle by distributing labile Zn^{2+}. ZIPs import Zn^{2+} into the cytosol, while ZnTs decrease $[Zn^{2+}]$ (labile Zn^{2+} concentrations) in the cytosol by either sequestering Zn^{2+} into organelles or secreting Zn^{2+} outside the cell.[4] Since both deficiency and excess of labile Zn^{2+} can cause cytotoxicity, many serious diseases are associated with dyshomeostasis of Zn^{2+}, such as growth retardation, immune deficiencies,[5] and Alzheimer's and Parkinson's diseases.[6,7] The disruption of zinc homeostasis could potentially disturb other transition metal ion homeostasis.[8] Therefore, quantitative clarification of Zn^{2+} dynamics at the organelle level can provide fundamental information to better understand the physiological roles of Zn^{2+} in individual organelles and assist in elucidating the chaotic networks of trace metal ions in cells.

Owing to its high sensitivity and non-invasiveness, fluorescence imaging is widely used to investigate biomolecules in living cells, tissues, and animals.[9] Fluorescent Zn^{2+} probes are generally classified into two types: small-molecule probes and genetically encoded probes. Since Zinquin was applied to investigate Zn^{2+} in cellular environments in 1993,[10] significant efforts have been made to further develop small-molecule fluorescent probes aiming to optimize the respective properties, such as Zn^{2+}-binding affinities, cell membrane permeability, and fluorescence wavelengths, for cellular applications.[11−18] Although several small-molecule probes have been widely used in zinc biology experiments, small-molecule probes are typically not suitable for the time-lapse monitoring of Zn^{2+} dynamics at the organelle level because they quickly diffuse in the cell and often leak from the cell to the medium.[19] The

Received: October 9, 2021
Accepted: February 24, 2022
Published: March 3, 2022

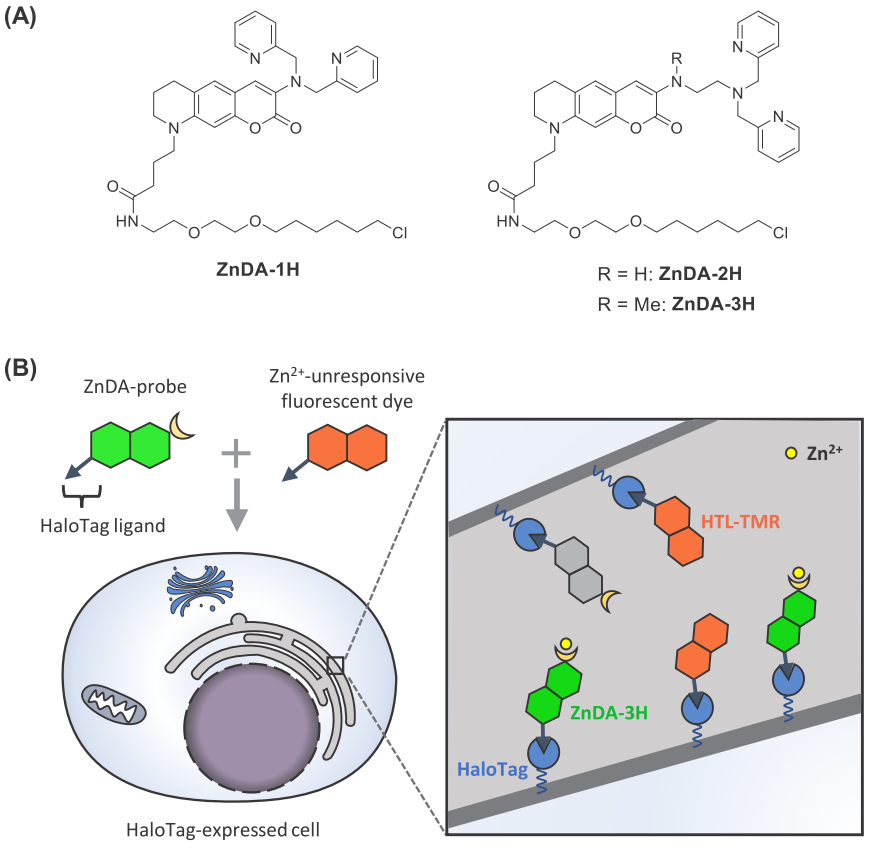

Figure 1. (A) Structures of ZnDA probes. (B) Illustration of the *in situ* standard quantification method.

incorporation of a targeting group is one approach to enable small-molecule probes to be localized at specific organelles. For example, triphenylphosphonium[20,21] and glibenclamide[22] can facilitate localization of the probe to the mitochondria and endoplasmic reticulum (ER), respectively. In addition, naphthalimide-based Zn^{2+} probes have been reported to selectively localize to particular organelle membranes by adjusting their lipophilicity.[23] However, the quantitative information about $[Zn^{2+}]$ in these organelles has been scarcely clarified by small-molecule probes.

On the other hand, genetically encoded Zn^{2+} sensors, also called fluorescent-protein (FP)-based probes, have been intensively developed in the past decades.[24] These kinds of probes can be specifically localized to target organelles by genetically fusing them with an appropriate localization signal peptide. This subcellular targetability is a key advantage over general small-molecule probes. Moreover, in contrast to small-molecule probes, the majority of which are intensiometric sensors, the ratiometric properties of FP-based probes make them more promising for the quantitative analysis of labile Zn^{2+} in organelles. However, the affinity of the FP-based probes for Zn^{2+} is considerably affected by variations in pH. For example, eCALWY exhibited a 10-fold difference in the dissociation constant (K_d) for Zn^{2+} between 0.63 nM at pH 7.1 and 60 pM at pH 7.8.[25] Another FP-based probe, eZinCh, has a higher pH sensitivity and showed a 100-fold K_d difference between 1.0 nM at pH 7.1 and 10 pM at pH 7.8.[26] Another limitation regarding the accurate quantification by FP-based Zn^{2+} probes is the small dynamic range (DR), which is the ratio of maximum and minimum signals. For example, the DRs of eCALWY and ZapCY1 are less than 2 and 3, respectively,[27] indicating that either a slight change in $[Zn^{2+}]$ in cells may not be detected or noise signals may largely affect the quantification results. Furthermore, oxidizing environments could reduce the DRs of the FP-based probes by formation of the disulfide-linked oligomers.[28] These susceptibilities of FP-based probes toward the surrounding environments would be one of the reasons for the largely different quantification results of $[Zn^{2+}]$ in the ER (0.9 pM[29] and 5.0 nM[25]) and mitochondria (0.14 pM[30] and 0.23 nM[25]). Therefore, there is still a high demand for the development of a more robust sensing platform for measuring $[Zn^{2+}]$, in addition to the need for an appropriate reevaluation of the exact labile Zn^{2+} distribution among various cellular compartments.

To achieve more accurate quantification of $[Zn^{2+}]$ in various organelles, the probes need to fulfill several requirements, including lower pH sensitivity, chemical robustness toward reactive oxygen species, greater DR, organelle targetability, and suitable Zn^{2+} affinity for $[Zn^{2+}]$ in target organelles. As a promising quantification technology for organellar labile Zn^{2+}, we recently developed a cell-permeable Zn^{2+} fluorescent probe, ZnDA-1H (Figure 1A),[31] which can be localized to subcellular compartments using a HaloTag labeling technology.[32] We achieved the quantification of the $[Zn^{2+}]$ in the Golgi apparatus ($[Zn^{2+}]_{Golgi}$) using the *in situ* standard quantification method (Figure 1B),[33] where ZnDA-1H and a Zn^{2+}-unresponsive red fluorescent HaloTag ligand (HTL-TMR), which is the internal standard, were used. The results indicated numerous $[Zn^{2+}]_{Golgi}$ in HeLa cells at nanomolar levels, which was substantially higher than those in the other examined cellular compartments, such as the ER and cytosol. However, $[Zn^{2+}]$ in these compartments could not be quantified because the concentration range of labile Zn^{2+} was lower than the detection limit of ZnDA-1H. Hence, in this study, we

https://doi.org/10.1021/acssensors.1c02153
ACS Sens. 2022, 7, 748−757

Table 1. Photophysical and Coordination Chemical Parameters of ZnDA Probes and the HaloTag-Conjugated Probes

	free probe[b]				Zn^{2+} complex[b]				K_d (nM)			
compound	$\lambda_{abs,max}$ (nm)	$\lambda_{em,max}$ (nm)	ε[d] (cm^{-1} M^{-1})	Φ	$\lambda_{abs,max}$ (nm)	$\lambda_{em,max}$ (nm)	ε[d] (cm^{-1} M^{-1})	Φ	pH 6.5	pH 7.0	pH 7.4	pH 8.0
compound 1	392	520	19,300	0.57								
ZnDA-1H[a]	409	518	21,700	0.028[c]	440	506	30,900	0.52[c]	3.2×10^2	2.9×10^2	2.4×10^2	
Halo−ZnDA-1H[a]	403	516	21,700	0.11[c]	438	507	27,600	0.91[c]	5.4×10^2	3.5×10^2	3.0×10^2	
ZnDA-2H	399	520	19,500	0.22[c]	417	506	24,000	0.56[c]			5.0	
Halo−ZnDA-2H	394	514	19,600	0.16	414	495	23,400	0.60	2.8	2.5	2.7	2.2
ZnDA-3H	407	508	19,200	0.029[c]	433	506	26,800	0.57[c]			0.16	
Halo−ZnDA-3H	402	504	20,600	0.11	431	503	27,600	0.77	0.37	0.083	0.082	0.11

[a]Data were obtained from ref 31. [b]Measured in HEPES buffer (pH 7.4). [c]Measured in HEPES buffer (pH 7.5). [d]Measured at $\lambda_{abs,max}$.

developed a series of ZnDA-probes with a higher affinity for Zn^{2+} (Figure 1A) and performed quantitative mapping of $[Zn^{2+}]$ in the nucleus, cytosol, mitochondria, and ER in living HeLa cells.

RESULTS AND DISCUSSION

Probe Design and Synthesis. A straightforward way to increase the Zn^{2+} affinity of the probe is to increase the coordination number of the chelator moiety. Therefore, in order to detect Zn^{2+} at nanomolar to picomolar levels, we designed a new probe, ZnDA-2H, with a higher-affinity Zn^{2+}-binding motif,[11,21,34,35] and its derivative, ZnDA-3H. This considered that the electron-donating property of the aromatic amino group at the 3-position of the coumarin may affect the affinity for Zn^{2+} and the photophysical properties (Figure 1A). As depicted in Scheme S1, ZnDA-2H was synthesized through reductive N-alkylation of the 3-amino group on the 3,7-diaminocoumarin dye with the ligand part and conjugation with a HaloTag amine (O2) ligand. ZnDA-3H was similarly synthesized with additional methylation on the 3-amino group before HaloTag ligand conjugation. After high performance liquid chromatography (HPLC) purification, the probes were characterized by ^{1}H nuclear magnetic resonance (NMR), ^{13}C NMR, and electrospray ionization mass spectrometry (ESI-MS). The probe concentrations were precisely determined using quantitative NMR. We further prepared HaloTag-bound ZnDA probes, Halo−ZnDA-2H and Halo−ZnDA-3H, which were the predicted active forms in live-cell imaging, in accordance with the procedures described in the Supporting Information.

Photophysical and Coordination Chemical Properties of Probes. The photophysical properties of both ZnDA-2H and ZnDA-3H were assessed using UV−vis absorption and fluorescence spectroscopy (Table 1). As the Zn^{2+} concentration increased, the absorption maxima of ZnDA-2H and ZnDA-3H red-shifted by forming Zn^{2+} complexes, with a slight increase in their absorbance (Figures S1A and S2A). Both probes showed Zn^{2+}-dependent fluorescence enhancement and comparable fluorescence quantum yield (Φ) in the Zn^{2+} complex state. In the absence of Zn^{2+}, ZnDA-3H showed almost no fluorescence (Φ = 0.029, pH 7.5), whereas ZnDA-2H showed weak fluorescence (Φ = 0.22, pH 7.5), indicating a much larger fluorescence enhancement of ZnDA-3H (40-fold) than that of ZnDA-2H (5.6-fold) (Figure 2A). Based on the fitted curve plot of the fluorescence intensity against Zn^{2+} concentration (Figure 2C), the K_d values of ZnDA-2H and ZnDA-3H for Zn^{2+} at pH 7.4 were determined to be 5.0 ± 0.6 and 0.16 ± 0.03 nM, respectively, thus indicating that these new probes are promising for detecting labile Zn^{2+} in target organelles such as the ER and mitochondria in concentration ranges from picomolar to submicromolar.

The pH sensitivity and metal ion selectivity of ZnDA-2H and ZnDA-3H were also investigated to validate their utility for quantitative imaging of labile Zn^{2+} in various organelles. Both probes did not show large fluorescence intensity changes with pH variations in the range of 5.5−8.0 (Figure 2D), suggesting their ability for more accurate $[Zn^{2+}]$ quantification at different pH levels in various organelles. The selectivity of the ZnDA probes toward Zn^{2+} over other biologically relevant metal ions present in mammalian cells was also examined (Figure 2E), whereby we used Na^+, K^+, Mg^{2+}, and Ca^{2+} at concentrations higher than, or close to, the physiological levels within mammalian cells.[36−38] The addition of a large quantity of these metal ions did not cause any significant fluorescence changes of the two probes, both in the presence and in the absence of Zn^{2+}. Thereafter, the fluorescence response toward other transition metal ions (namely, Mn^{2+}, Fe^{3+}, Fe^{2+}, Co^{2+}, Ni^{2+}, Cu^{2+}, Cu^+, and Cd^{2+}) was investigated. Cd^{2+}, which has a similar electronic configuration (d^{10}) as Zn^{2+}, showed a marked increase in the fluorescence intensity of both probes in the absence of Zn^{2+}. Cu^{2+} and Cu^+ showed a quenching effect on both probes, even in the presence of the same concentration of Zn^{2+}, suggesting that both probes had a higher affinity for copper ions than Zn^{2+}. Except for Cd^{2+}, Cu^{2+}, and Cu^+, other transition metal ions had little effect on the fluorescence of both probes.

Thereafter, we investigated the fluorescence quenching mechanism of Zn^{2+}-free ZnDA probes. In our previous study,[31] density functional theory (DFT) calculations on ZnDA-1H indicated that the fluorescence quenching of Zn^{2+}-free ZnDA-1H was not caused by photoinduced electron transfer (PeT) from the pyridine moieties. In this study, ZnDA-2H and ZnDA-3H had one additional aliphatic amino group in their chelator parts, which may have caused fluorescence quenching by PeT in the absence of Zn^{2+}. The pK_a values of the aliphatic amino groups of ZnDA-2H and ZnDA-3H were predicted to be 5.9 and 6.5, respectively (Figure S4), suggesting that some fractions of the aliphatic amino groups in ZnDA-2H and ZnDA-3H were protonated in solutions where the pH was less than 6.0. However, the fluorescence measurements in different pH solutions (Figure 2D) showed that the fluorescence intensity was weak and scarcely changed in the pH range from 5.5 to 8.0 for both ZnDA-2H and ZnDA-3H in the absence of Zn^{2+}. These results suggest that PeT is not the dominant mechanism for the fluorescence quenching of ZnDA-2H and ZnDA-3H in the Zn^{2+}-free states.

https://doi.org/10.1021/acssensors.1c02153
ACS Sens. 2022, 7, 748−757

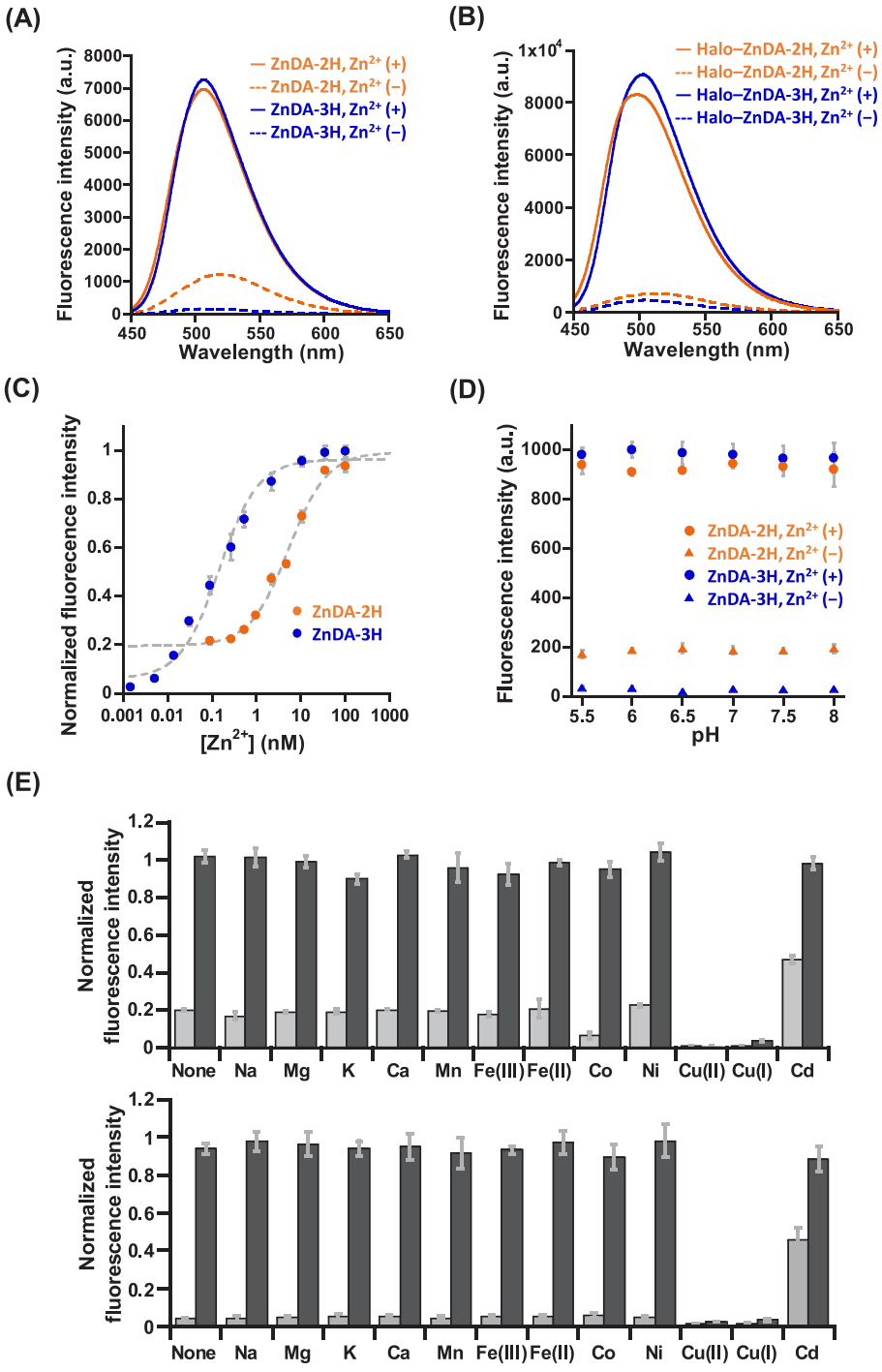

Figure 2. Photophysical and coordination chemical properties of ZnDA-2H (orange) and ZnDA-3H (blue). (A, B) Fluorescence spectra of 0.5 μM ZnDA-2H (λ_{ex} = 420 nm) (A), ZnDA-3H (λ_{ex} = 430 nm) (A), Halo−ZnDA-2H (λ_{ex} = 420 nm) (B), and Halo−ZnDA-3H (λ_{ex} = 430 nm) (B) without and with 20 μM Zn^{2+} in 100 mM HEPES buffer (I = 0.1 M ($NaNO_3$), pH 7.4). (C) Fluorescence intensity of ZnDA-2H and ZnDA-3H as a function of [Zn^{2+}] at pH 7.4. Error bars represent SD (n = 3). (D) Fluorescence intensity of the ZnDA probes without and with 1 μM Zn^{2+} at various pHs. Error bars represent SD (n = 3). (E) Metal ion selectivity of ZnDA-2H (top) and ZnDA-3H (bottom). The fluorescence intensity of ZnDA-2H and ZnDA-3H (0.1 μM) was measured without (light gray bars) and with 1 μM Zn^{2+} (dark gray bars) in the presence of various metal ions ([Na^+], [Mg^{2+}], and [Ca^{2+}] = 10 mM, [K^+] = 150 mM, [Mn^{2+}], [Fe^{3+}], [Fe^{2+}], [Co^{2+}], [Ni^{2+}], [Cu^{2+}], [Cu^+], and [Cd^{2+}] = 1 μM) in 100 mM HEPES buffer (pH 7.4). Error bars represent SD (n = 3).

Another plausible mechanism for the quenching is a nonradiative relaxation through twisted intramolecular charge transfer (TICT), which has been well studied regarding 7-aminocoumarins.[39] The transition to the TICT state is more likely to occur in polar solvents with an increasing number of substituents on the aromatic amino group, resulting in a decrease in the fluorescence intensity.[39−41] The solvatochromic behaviors of the four compounds were investigated in a homologous series of alcohols (Table S1 and Figure S5A,B). In Figure S5B, Φ of ZnDA-2H gradually decreased as the solvent polarity function Δf[42] increased and drastically decreased at Δf = 0.31. This biphasic change of Φ depending on the solvent

https://doi.org/10.1021/acssensors.1c02153
ACS Sens. 2022, 7, 748−757

polarity is a common characteristic of TICT, as seen in 7-diethylaminocoumarin.[43] On the other hand, ZnDA-1H and ZnDA-3H showed low Φ even in a low-polarity solvent (Δf = 0.24). To further verify whether the low Φ of the ZnDA probes is due to the TICT mechanism, the viscosity sensitivity of the probe fluorescence was assessed. The fluorescence intensity of ZnDA-1H and ZnDA-3H in ethylene glycol largely decreased at higher temperatures, i.e., at lower viscosities, with a small shift in the emission maxima (Figure S5C,D). ZnDA-2H showed the same trend with a moderate viscosity-dependent fluorescence increase, whereas the fluorescence intensity of compound **1** (Scheme S1) showed a lower viscosity dependence. These results suggest that the non-radiative decay of ZnDA probes with a 3-alkylaminocoumarin moiety was suppressed in highly viscous solutions due to the restriction of the C−N bond rotation that induces TICT. Thus, all data suggest that the fluorescence quenching of ZnDA probes is based on the TICT mechanism.

Since ZnDA probes bind to the locally expressed HaloTag proteins in live-cell studies, it is important to understand the Zn^{2+} binding and photophysical properties of HaloTag-bound probes, Halo−ZnDA-2H and Halo−ZnDA-3H. With increasing Zn^{2+} concentrations from 0 to 50 μM, the absorption spectra of Halo−ZnDA-2H and Halo−ZnDA-3H showed a red-shift from 394 to 414 nm and from 402 to 431 nm, respectively, with an isosbestic point and a slight increase in the absorbance (Figures S1C and S2C). The Zn^{2+}-binding stoichiometries of both probes were confirmed to be 1:1 by plotting the absorbance changes against the concentration ratio of Zn^{2+} and the probes (Figures S1D and S2D). The fluorescence enhancement of Halo−ZnDA-2H and Halo−ZnDA-3H upon binding with Zn^{2+} was 11- and 20-fold, respectively (Figure 2B). The Φ of Halo−ZnDA-3H in the absence of Zn^{2+} was 0.11 at pH 7.4, which was higher than that of ZnDA-3H (Φ = 0.029, pH 7.5). This increase suggests that the quenching process is insufficient in Halo−ZnDA-3H, which may be due to the location of the coumarin fluorophore of ZnDA-3H being within a less polar environment around the HaloTag protein surface.

Thereafter, the K_d values of Halo−ZnDA-2H and Halo−ZnDA-3H for Zn^{2+} were estimated by fluorescence measurements (Figure S3 and Table 1). As various organelles show characteristic pH ranges, we also estimated the K_d values under several pH conditions. While the K_d values of Halo−ZnDA-2H minimally changed (2.8 nM at pH 6.5, 2.5 nM at pH 7.0, and 2.2 nM at pH 8.0), those of Halo−ZnDA-3H were moderately affected by pH (0.37 nM at pH 6.5, 0.083 nM at pH 7.0, and 0.11 nM at pH 8.0) (Figure S3 and Table 1). Nevertheless, the change in K_d of Halo−ZnDA-3H between pH 6.5 and pH 7.4 is 4.5-fold, indicating that Halo−ZnDA-3H has a substantially lower sensitivity toward pH variations than the reported FP-based probes.[25,26]

Organelle-Targeting Properties of Probes. To confirm the subcellular targeting properties of both ZnDA-2H and ZnDA-3H, we performed co-localization experiments with fluorescent organelle markers. HeLa cells were used for all cell experiments and were transfected with various plasmids encoding HaloTag, fused with a specific localization signal, namely, SV40 T-antigen nuclear localization signal (NLS) for the nucleus, a subunit VIII of human cytochrome *c* oxidase (COX8) for the mitochondria, and C-terminal KDEL sequence for the ER, or without any signal peptide for the cytosol. Transfected HeLa cells were co-incubated with either ZnDA-2H or ZnDA-3H and an organelle marker (i.e., Hoechst 33342 for the nucleus, MitoTracker Orange for the mitochondria, and ER-Tracker Red for the ER). Fluorescence images were taken by confocal laser scanning microscopy (CLSM) after adding Zn^{2+}/pyrithione (ZPT) to obtain the maximum fluorescence intensity of ZnDA probes bound to Zn^{2+}. Both ZnDA-2H (Figure S6) and ZnDA-3H (Figure 3)

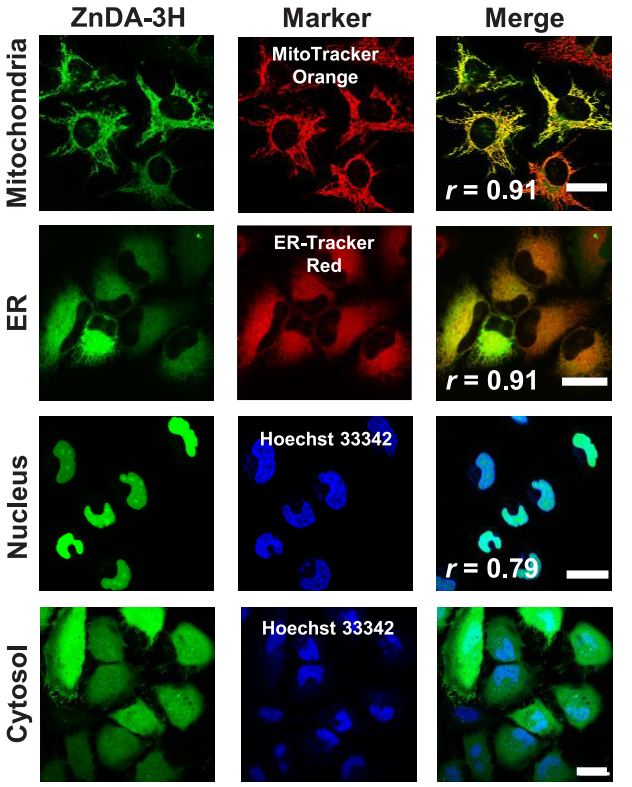

Figure 3. Confocal microscopy images of HeLa cells using ZnDA-3H (0.25 μM) and organelle markers. HaloTag proteins were expressed in the mitochondria, ER, nucleus, and cytosol. MitoTracker Orange, ER-Tracker Red, and Hoechst 33342 were used as organelle markers. The images were acquired after the addition of ZPT. *r* indicates Pearson's correlation coefficient. Scale bars = 30 μm.

were clearly localized in the target subcellular compartments. The organelle localization of ZnDA probes was quantitatively assessed by Pearson's correlation coefficient (*r*) for co-localization with the fluorescent signals of the organelle markers. Both probes showed high co-localization with the marker signals of the target organelles, namely, the mitochondria, *r* = 0.90 (ZnDA-2H) and 0.91 (ZnDA-3H); the ER, *r* = 0.87 (ZnDA-2H) and 0.91 (ZnDA-3H); and the nucleus, *r* = 0.81 (ZnDA-2H) and 0.79 (ZnDA-3H). Minimal off-target probe accumulation was observed in HaloTag-expressing cells. These findings indicate that both ZnDA-2H and ZnDA-3H can be precisely localized to the target cellular compartments using HaloTag labeling technology.

Quantification of [Zn^{2+}] in Various Cellular Compartments. Based on the *in situ* standard quantification method via simultaneous labeling of HaloTag with a Zn^{2+}-unresponsive HTL-TMR and a ZnDA probe (Figure 1B), the fluorescence signal deviation due to either the focal plane drift or the cell morphological change during imaging can be calibrated by calculating the fluorescence ratio of the ZnDA probe to the HTL-TMR ($R = F_{ZnDA}/F_{TMR}$).[31,33] The fluorescence inten-

https://doi.org/10.1021/acssensors.1c02153
ACS Sens. 2022, 7, 748−757

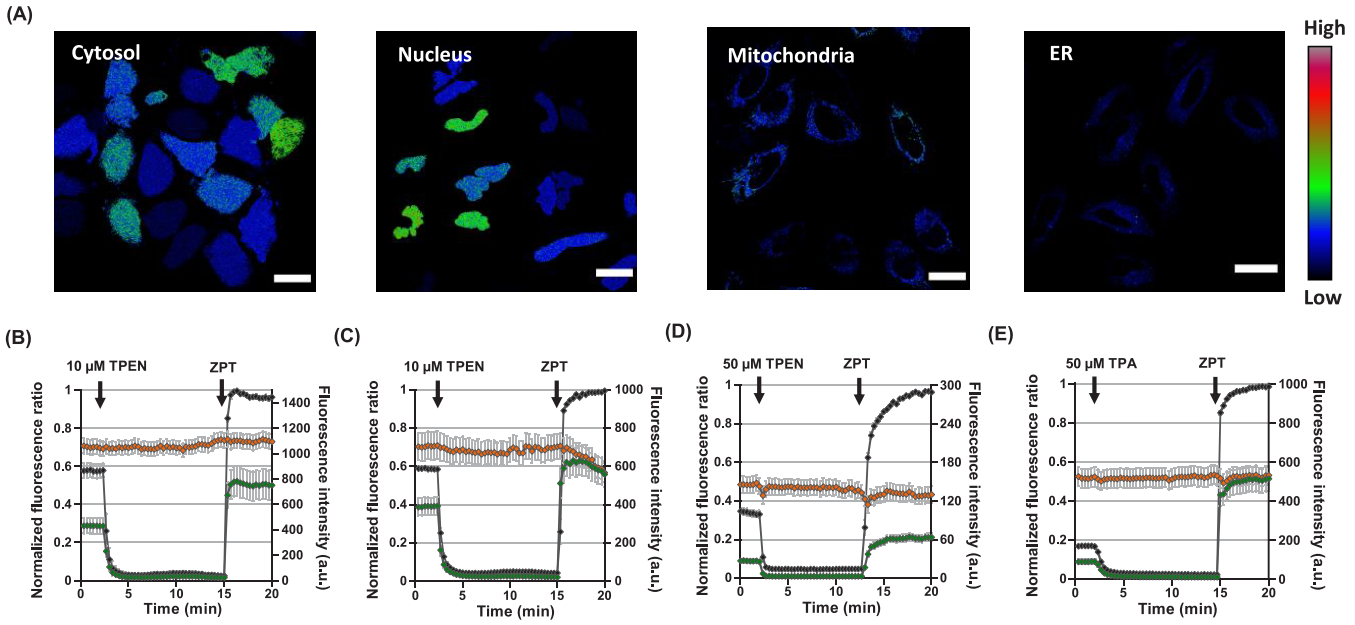

Figure 4. (A) Pseudocolor fluorescence ratio images of ZnDA-3H/HTL-TMR at the steady state in each organelle. Scale bars = 30 μm. (B–E) Time course of the *in situ* calibration of the normalized fluorescence ratio (black) and fluorescence intensity of ZnDA-3H (green) and HTL-TMR (orange) for $[Zn^{2+}]$ quantification in cytosol (B), nucleus (C), mitochondria (D), and ER (E). Error bars represent SEM (B, n = 35; C, n = 33; D, n = 27; E, n = 26).

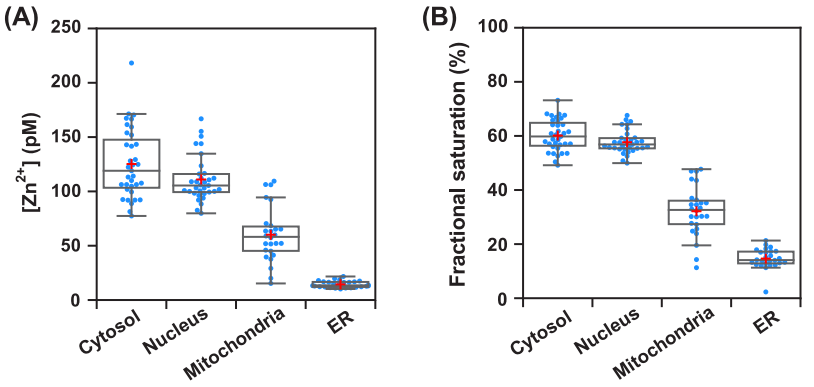

Figure 5. Quantitative mapping of organellar $[Zn^{2+}]$ by using ZnDA-3H (A) and fractional saturation of ZnDA-3H at the steady state (B) in various organelles. Red plus symbols represent the mean values.

sities in both green and red channels were recorded for 3 min at the steady state, followed by the *in situ* calibration by the sequential addition of Zn^{2+}-depleting chelator and ZPT to determine the minimum and maximum R values, R_{min} and R_{max}, respectively, in the living cells. R was normalized to R_{max} to estimate the fractional saturation (FS) of the ZnDA probes. The FS at the steady state (FS_{ss}) can be estimated using the following equation

$$FS_{ss} = (R_{ss} - R_{min})/(R_{max} - R_{min})$$

$[Zn^{2+}]$ at the steady state can be calculated using the following equation

$$[Zn^{2+}] = K_d(R_{ss} - R_{min})/(R_{max} - R_{ss}) = K_d FS_{ss}/(1 - FS_{ss})$$

by using the K_d value estimated *in vitro* for the Halo–ZnDA probe at an appropriate pH in the target cellular compartment (Table 1).

We performed $[Zn^{2+}]$ quantification using ZnDA-3H with time-lapse CLSM imaging in living HeLa cells (Figure 4). Stepwise treatment with 10 μM TPEN and ZPT (50 μM Zn^{2+}/5 μM pyrithione) rapidly and sufficiently induced the ZnDA-3H fluorescence signals to reach a minimum level, followed by a maximum level in the cytosol and nucleus (Figure 4B,C). By using the K_d value (0.082 nM) of Halo–ZnDA-3H at pH 7.4, the $[Zn^{2+}]$ in the cytosol ($[Zn^{2+}]_{cyto}$) and $[Zn^{2+}]$ in the nucleus ($[Zn^{2+}]_{nuc}$) were estimated to be 0.13 nM (FS_{ss} = 60%) and 0.11 nM (FS_{ss} = 58%), respectively (Figure 5). ZnDA-2H was also used for the $[Zn^{2+}]$ quantification, and the $[Zn^{2+}]_{cyto}$ and $[Zn^{2+}]_{nuc}$ were estimated to be 0.22 nM (FS_{ss} = 6.0%) and 0.17 nM (FS_{ss} = 5.7%), respectively (Figure S7A,B, and Table S3).

The estimated $[Zn^{2+}]_{cyto}$ and $[Zn^{2+}]_{nuc}$ values are consistent with the previously reported and widely accepted values at hundreds of picomolar levels.[44,45] A slight increase in the fluorescence signals of both ZnDA-3H and HTL-TMR was observed outside the nucleus after ZPT addition in the 250 ng plasmid condition (Figure S8), which might be due to the diffusion of Halo-NLS proteins from the nucleus to the cytosol

https://doi.org/10.1021/acssensors.1c02153
ACS Sens. 2022, 7, 748–757

by excessive Zn^{2+}. This translocation caused a decrease in the HTL-TMR and ZnDA-3H signals after ZPT addition (Figure 4C). In the 50 ng plasmid condition, ZPT addition did not induce Halo-NLS diffusion from the nucleus. To investigate the effect of Halo-NLS expression on Zn^{2+} concentration in the nucleus, we performed $[Zn^{2+}]_{nuc}$ quantification under 50 ng Halo-NLS plasmid conditions (Figure S9). There was almost no difference in the estimated $[Zn^{2+}]_{nuc}$ values between the 250 and 50 ng plasmid conditions. This result suggests that the expressed HaloTag proteins do not significantly affect steady-state Zn^{2+} levels. The lack of difference in the estimated $[Zn^{2+}]$ values between the two conditions also indicates that this phenomenon is not critical for our quantification method, probably because the R values can be appropriately compensated for by the simultaneous change in the HTL-TMR fluorescence intensity.

As shown in Figure S10, 10 μM TPEN treatment was not sufficient to achieve the Zn^{2+}-depleted state in the ER and mitochondria, likely due to the moderate membrane permeability of TPEN. Therefore, *in situ* calibration conditions were optimized to provide more stable Zn^{2+}-depletion states in these organelles. Tris(2-pyridylmethyl)amine (TPA) was also tested for Zn^{2+} depletion due to higher membrane permeability and lower cell toxicity.[46] Finally, treatment with 50 μM TPA and 50 μM TPEN for the ER and mitochondria, respectively, was found to induce a sufficient and rapid decrease of the ZnDA-3H fluorescence signals in the ER and the mitochondria (Figure 4D,E). The $[Zn^{2+}]$ in the ER ($[Zn^{2+}]_{ER}$) and $[Zn^{2+}]$ in the mitochondria ($[Zn^{2+}]_{mito}$) were determined to be 14 pM (FS_{ss} = 15%) and 60 pM (FS_{ss} = 29%), respectively (Figure 5). On the other hand, the fluorescence signals of ZnDA-2H in the ER and the mitochondria were not significantly decreased by TPEN treatment to estimate the reliable steady-state $[Zn^{2+}]$ (Figure S7C,D). These results by ZnDA-2H also clearly indicate that the $[Zn^{2+}]$ values in the ER and mitochondria were lower than those in the cytosol and nucleus.

To ascertain whether *in situ* calibration was performed while maintaining cell health, we also investigated the cytotoxicity of ZPT using the MTT assay. Figure S11A indicates that almost all cells were viable 5 min after the addition of ZPT, suggesting that cell health was well maintained during the time required to obtain the R_{max} values. Moreover, the cell viability under the conditions that mimic those for *in situ* calibration, in which TPEN or TPA was used in addition to ZPT, showed that more than 90% of the cells survived 6 min after adding ZPT (Figure S11B). These findings indicate that the $[Zn^{2+}]$ values were quantified under appropriate conditions without substantial cytotoxicity due to ZPT and the Zn^{2+} chelators. However, the longer incubation time did reduce cell viability to 70% or lower due to the intrinsic cytotoxicity of ZPT.[47−49]

Considering the high Zn^{2+}-binding affinity of ZnDA-3H, which might disturb the homeostasis of the labile Zn^{2+} pool in the examined organelles, the effect of the ZnDA-3H concentration on the $[Zn^{2+}]_{ER}$ was evaluated. The results showed no significant difference in the $[Zn^{2+}]_{ER}$ estimated using different concentrations of ZnDA-3H in the labeling conditions from 50 nM to 1.0 μM (Figure S12). This result excludes the possibility that the targeted ZnDA-3H decreased the steady-state labile Zn^{2+} concentration in the ER. Thus, it is reasonable to consider that the quantification data reflect the physiological values of the steady-state $[Zn^{2+}]_{ER}$ under our experimental conditions. In addition, to verify whether the labeling ratio of HaloTag proteins with ZnDA-3H and HTL-TMR in a target organelle affects the resulting values of $[Zn^{2+}]$, we statistically analyzed the data obtained by ZnDA-3H in each organelle. The results indicate that the estimated $[Zn^{2+}]$ values were not correlated with either the fluorescence intensities of either probe or R_{max} (Figure S13). We also investigated the sub-organellar distribution of the two fluorophores and evaluated the deviation in the estimated $[Zn^{2+}]_{nuc}$ in a single nucleus (Figure S14). The SD of $[Zn^{2+}]$ calculated from 15 sub-nuclear microregions of four examined cells ranged from 4.7 to 8.9 pM (5.9−10% of the mean values). Assuming that the intranuclear labile Zn^{2+} is equilibrated, these distributions indicate the precision of our quantification method for a sub-organellar microregion. In contrast, the single-cell level $[Zn^{2+}]_{nuc}$ was distributed with a larger SD (21.0 pM, 18.9% of the mean value, n = 33 cells, Table S4). This was expected due to the individuality of living cells.

In this study, the K_d values at specific pH levels for the cytosol (pH 7.4), nucleus (pH 7.4), ER (pH 7.4), and mitochondria (pH 8.0) were used for subcellular $[Zn^{2+}]$ quantification. Although more precise quantification of $[Zn^{2+}]$ would be achieved with simultaneous pH quantification, the K_d values of ZnDA-3H at pH 7.0 and pH 7.4 were almost the same (Table S3), and the lower pH sensitivity of ZnDA-3H indicated the robustness of this quantification method in living cells. We quantified the zinc concentrations in the cytosol and nucleus by using ZnDA-2H and ZnDA-3H, and the $[Zn^{2+}]_{cyto}$ and $[Zn^{2+}]_{nuc}$ estimated with both probes fell within the range of 0.1−0.2 nM. Although $[Zn^{2+}]_{mito}$ and $[Zn^{2+}]_{ER}$ were out of the detection range of ZnDA-2H, ZnDA-3H was suitable for quantification with FS in the range of 10−90%. Our estimated $[Zn^{2+}]_{mito}$ (60 pM) was similar to the $[Zn^{2+}]_{mito}$ of NIH3T3 cells reported by DQZn2 (72 pM).[20] In contrast, $[Zn^{2+}]_{mito}$ previously estimated by FP-based probes differed greatly from each other, ranging from 0.14 to 230 pM.[25,30] All of these results indicate that small-molecule−protein hybrid probes provided more robust quantification data, especially for organellar Zn^{2+} concentrations.

Another factor that can influence the quantification results is the effect of other metal ions. In the *in vitro* metal ion selectivity assay (Figure 2E), no other metal ions except copper ions affected the fluorescence signals of ZnDA-3H. Although the intracellular labile copper ion concentrations ($[Cu^{+}]$ and $[Cu^{2+}]$) are thought to be extremely low,[50] those in organelles have not yet been clarified. Therefore, we cannot exclude the underestimation of $[Zn^{2+}]$ by the partial coordination of ZnDA probes in some organelles until the clarification of subcellular labile copper ion distributions. However, by virtue of a lower pH dependence of K_d values and the sub-nM level Zn^{2+} affinity of ZnDA-3H, this study provided the quantitative data concerning subcellular Zn^{2+} distributions in HeLa cells as $[Zn^{2+}]_{ER} < [Zn^{2+}]_{mito} < [Zn^{2+}]_{cyto} \sim [Zn^{2+}]_{nuc}$. Such an organelle-level bias in Zn^{2+} concentration is likely to be involved in the minute regulation of cellular functions. A recent study showed that the chaperone protein ERp44 in the ER and Golgi apparatus has an apparent K_d for Zn^{2+} of 135 nM at pH 7.2.[51] Our quantification results suggest that, whereas ERp44 primarily exists in a Zn^{2+}-free form in the ER ($[Zn^{2+}]$ = 14 pM), some ERp44 form a Zn^{2+} complex in the Golgi apparatus ($[Zn^{2+}]$ = 25 nM[31]). Thus, it is likely that Zn^{2+} is an essential mediator for modulating the physiological functions of various Zn^{2+}-coordinating proteins such as ERp44.

Compared with FRET-type small-molecule probes, our method, which uses a sensing probe and a standard

https://doi.org/10.1021/acssensors.1c02153
ACS Sens. 2022, 7, 748−757

fluorophore, has the following advantages: no intramolecular interference between the two fluorophores, easier probe modifiability owing to its simple structure, and a large dynamic range of fluorescence with a bright fluorescent sensor. Furthermore, in principle, it can be used to detect a variety of targets by simply changing the sensor site. However, the quantification protocol is complex. Therefore, we recognize the importance of developing ratiometric probes in the future.

CONCLUSIONS

In summary, we developed two novel fluorescent probes with high affinity for Zn^{2+}, namely, ZnDA-2H (K_d = 5.0 nM) and ZnDA-3H (K_d = 0.16 nM). Both probes showed high Zn^{2+} selectivity and nearly pH-independent fluorescence at various pH levels (5.5−8.0), suggesting that these two probes can be used for monitoring cellular Zn^{2+} fluctuations without serious disturbance from pH changes in organelles. We also investigated the fluorescence quenching mechanism of the free ZnDA probes, and the data indicated that binding with Zn^{2+} could hinder the transition to the TICT state in the excited state. CLSM imaging revealed that both ZnDA-2H and ZnDA-3H could be precisely localized in the cytosol, nucleus, ER, and mitochondria using HaloTag labeling technology. Owing to the suitably high Zn^{2+} affinity of ZnDA-3H, we quantitatively mapped subcellular $[Zn^{2+}]$ in live HeLa cells by utilizing the *in situ* quantification method via co-labeling with Zn^{2+}-unresponsive HTL-TMR. In all tested organelles, the FS values of ZnDA-3H were in the range of 10−90%, indicating that ZnDA-3H is appropriate for $[Zn^{2+}]$ quantification. The results indicated that $[Zn^{2+}]$ values in the cytosol (0.13 nM) and nucleus (0.11 nM) were higher than those in the mitochondria (60 pM) and ER (14 pM). Considering the advantages, such as robustness to pH change and large DR, of ZnDA-3H and the other two probes ZnDA-1H and ZnDA-2H, which have different K_d values for Zn^{2+}, we believe that a series of ZnDA probes can be widely used to quantify $[Zn^{2+}]$ in living cells and could be useful for elucidating the physiological roles of subcellular Zn^{2+} dynamics.

ASSOCIATED CONTENT

Supporting Information

The Supporting Information is available free of charge at https://pubs.acs.org/doi/10.1021/acssensors.1c02153.

Materials and instruments, synthesis and analytical data of new compounds, coordination and photophysical properties of the probes, and live-cell imaging data (PDF)

AUTHOR INFORMATION

Corresponding Author

Shin Mizukami − *Graduate School of Life Sciences and Institute of Multidisciplinary Research for Advanced Materials, Tohoku University, Sendai, Miyagi 980-8577, Japan; Department of Chemistry, Faculty of Science, Tohoku University, Sendai, Miyagi 980-8578, Japan; AMED-CREST, Japan Agency for Medical Research and Development, Tokyo 100-0004, Japan;* orcid.org/0000-0002-2292-8606; Email: shin.mizukami@tohoku.ac.jp

Authors

Rong Liu − *Graduate School of Life Sciences, Tohoku University, Sendai, Miyagi 980-8577, Japan*

Toshiyuki Kowada − *Graduate School of Life Sciences and Institute of Multidisciplinary Research for Advanced Materials, Tohoku University, Sendai, Miyagi 980-8577, Japan; Department of Chemistry, Faculty of Science, Tohoku University, Sendai, Miyagi 980-8578, Japan;* orcid.org/0000-0002-6623-6505

Yuyin Du − *Department of Chemistry, Faculty of Science, Tohoku University, Sendai, Miyagi 980-8578, Japan*

Yuta Amagai − *Institute of Multidisciplinary Research for Advanced Materials, Tohoku University, Sendai, Miyagi 980-8577, Japan;* orcid.org/0000-0002-2999-4622

Toshitaka Matsui − *Graduate School of Life Sciences and Institute of Multidisciplinary Research for Advanced Materials, Tohoku University, Sendai, Miyagi 980-8577, Japan; Department of Chemistry, Faculty of Science, Tohoku University, Sendai, Miyagi 980-8578, Japan*

Kenji Inaba − *Graduate School of Life Sciences and Institute of Multidisciplinary Research for Advanced Materials, Tohoku University, Sendai, Miyagi 980-8577, Japan; Department of Chemistry, Faculty of Science, Tohoku University, Sendai, Miyagi 980-8578, Japan; AMED-CREST, Japan Agency for Medical Research and Development, Tokyo 100-0004, Japan;* orcid.org/0000-0001-8229-0467

Complete contact information is available at: https://pubs.acs.org/10.1021/acssensors.1c02153

Author Contributions

R.L., T.K., K.I., and S.M. constructed the research strategy. R.L., T.K., and Y.D. synthesized and characterized the fluorescent probe. R.L., T.K., and T.M. constructed the plasmids. R.L. performed the cell imaging experiments. R.L., T.K., and S.M. wrote the initial draft of the manuscript, and Y.A., T.M., and K.I. joined to finalize the manuscript.

Notes

The authors declare no competing financial interest.

ACKNOWLEDGMENTS

This work was supported by JSPS KAKENHI (Nos. JP18H02102, JP19K22241, JP20K05702, and JP21H05252) and by the Takeda Science Foundation, the Nakatani Foundation, AMED-CREST (21gm1410006h0001), and the "Dynamic Alliance for Open Innovation Bridging Human, Environment and Materials" Research Program in the "Network Joint Research Center for Materials and Devices". We thank Tagen Central Analytical Facility for providing NMR and MS instruments.

REFERENCES

(1) Maret, W. Zinc Biochemistry: From a Single Zinc Enzyme to a Key Element of Life. *Adv. Nutr.* **2013**, *4*, 82−91.

(2) Maret, W. Zinc Proteomics and the Annotation of the Human Zinc Proteome. *Pure Appl. Chem.* **2008**, *80*, 2679−2687.

(3) Krężel, A.; Maret, W. The Biological Inorganic Chemistry of Zinc Ions. *Arch. Biochem. Biophys.* **2016**, *611*, 3−19.

(4) Kambe, T.; Tsuji, T.; Hashimoto, A.; Itsumura, N. The Physiological, Biochemical, and Molecular Roles of Zinc Transporters in Zinc Homeostasis and Metabolism. *Physiol. Rev.* **2015**, *95*, 749−784.

(5) Haase, H.; Rink, L. Functional Significance of Zinc-Related Signaling Pathways in Immune Cells. *Annu. Rev. Nutr.* **2009**, *29*, 133−152.

(6) Frederickson, C. J.; Koh, J. Y.; Bush, A. I. The Neurobiology of Zinc in Health and Disease. *Nat. Rev. Neurosci.* **2005**, *6*, 449−462.

(7) Sensi, S. L.; Paoletti, P.; Bush, A. I.; Sekler, I. Zinc in the Physiology and Pathology of the CNS. *Nat. Rev. Neurosci.* **2009**, *10*, 780−791.
(8) Krężel, A.; Maret, W. The Functions of Metamorphic Metallothioneins in Zinc and Copper Metabolism. *Int. J. Mol. Sci.* **2017**, *18*, 1237.
(9) Chen, Y.; Bai, Y.; Han, Z.; He, W.; Guo, Z. Photoluminescence Imaging of Zn^{2+} in Living Systems. *Chem. Soc. Rev.* **2015**, *44*, 4517−4546.
(10) Zalewski, P. D.; Forbes, I. J.; Betts, W. H. Correlation of Apoptosis with Change in Intracellular Labile Zn(II) Using Zinquin [(2-Methyl-8-*p*-Toluenesulphonamido-6-Quinolyloxy)Acetic Acid], a New Specific Fluorescent Probe for Zn(II). *Biochem. J.* **1993**, *296*, 403−408.
(11) Hirano, T.; Kikuchi, K.; Urano, Y.; Higuchi, T.; Nagano, T. Highly Zinc-Selective Fluorescent Sensor Molecules Suitable for Biological Applications. *J. Am. Chem. Soc.* **2000**, *122*, 12399−12400.
(12) Rivera-Fuentes, P.; Wrobel, A. T.; Zastrow, M. L.; Khan, M.; Georgiou, J.; Luyben, T. T.; Roder, J. C.; Okamoto, K.; Lippard, S. J. A Far-Red Emitting Probe for Unambiguous Detection of Mobile Zinc in Acidic Vesicles and Deep Tissue. *Chem. Sci.* **2015**, *6*, 1944−1948.
(13) Kiyose, K.; Kojima, H.; Urano, Y.; Nagano, T. Development of a Ratiometric Fluorescent Zinc Ion Probe in Near-Infrared Region, Based on Tricarbocyanine Chromophore. *J. Am. Chem. Soc.* **2006**, *128*, 6548−6549.
(14) Kim, J. J.; Hong, J.; Yu, S.; You, Y. Deep-Red-Fluorescent Zinc Probe with a Membrane-Targeting Cholesterol Unit. *Inorg. Chem.* **2020**, *59*, 11562−11576.
(15) Walkup, G. K.; Burdette, S. C.; Lippard, S. J.; Tsien, R. Y. A New Cell-Permeable Fluorescent Probe for Zn^{2+}. *J. Am. Chem. Soc.* **2000**, *122*, 5644−5645.
(16) Taki, M.; Wolford, J. L.; O'Halloran, T. V. Emission Ratiometric Imaging of Intracellular Zinc: Design of a Benzoxazole Fluorescent Sensor and Its Application in Two-Photon Microscopy. *J. Am. Chem. Soc.* **2004**, *126*, 712−713.
(17) Komatsu, K.; Kikuchi, K.; Kojima, H.; Urano, Y.; Nagano, T. Selective Zinc Sensor Molecules with Various Affinities for Zn^{2+}, Revealing Dynamics and Regional Distribution of Synaptically Released Zn^{2+} in Hippocampal Slices. *J. Am. Chem. Soc.* **2005**, *127*, 10197−10204.
(18) Xu, H.; Zhu, C.; Chen, Y.; Bai, Y.; Han, Z.; Yao, S.; Jiao, Y.; Yuan, H.; He, W.; Guo, Z. A FRET-Based Fluorescent Zn^{2+} Sensor: 3D Ratiometric Imaging, Flow Cytometric Tracking and Cisplatin-Induced Zn^{2+} Fluctuation Monitoring. *Chem. Sci.* **2020**, *11*, 11037−11041.
(19) Hessels, A. M.; Taylor, K. M.; Merkx, M. Monitoring Cytosolic and ER Zn^{2+} in Stimulated Breast Cancer Cells Using Genetically Encoded FRET Sensors. *Metallomics* **2016**, *8*, 211−217.
(20) Xue, L.; Li, G.; Yu, C.; Jiang, H. A Ratiometric and Targetable Fluorescent Sensor for Quantification of Mitochondrial Zinc Ions. *Chem.Eur. J.* **2012**, *18*, 1050−1054.
(21) Masanta, G.; Lim, C. S.; Kim, H. J.; Han, J. H.; Kim, H. M.; Cho, B. R. A Mitochondrial-Targeted Two-Photon Probe for Zinc Ion. *J. Am. Chem. Soc.* **2011**, *133*, 5698−5700.
(22) Fang, L.; Trigiante, G.; Crespo-Otero, R.; Hawes, C. S.; Philpott, M. P.; Jones, C. R.; Watkinson, M. Endoplasmic Reticulum Targeting Fluorescent Probes to Image Mobile Zn^{2+}. *Chem. Sci.* **2019**, *10*, 10881−10887.
(23) Fang, H.; Geng, S.; Hao, M.; Chen, Q.; Liu, M.; Liu, C.; Tian, Z.; Wang, C.; Takebe, T.; Guan, J. L.; Chen, Y.; Guo, Z.; He, W.; Diao, J. Simultaneous Zn^{2+} Tracking in Multiple Organelles Using Super-Resolution Morphology-Correlated Organelle Identification in Living Cells. *Nat. Commun.* **2021**, *12*, 109.
(24) Carter, K. P.; Young, A. M.; Palmer, A. E. Fluorescent Sensors for Measuring Metal Ions in Living Systems. *Chem. Rev.* **2014**, *114*, 4564−4601.
(25) Chabosseau, P.; Tuncay, E.; Meur, G.; Bellomo, E. A.; Hessels, A.; Hughes, S.; Johnson, P. R. V.; Bugliani, M.; Marchetti, P.; Turan, B.; Lyon, A. R.; Merkx, M.; Rutter, G. A. Mitochondrial and ER-Targeted ECALWY Probes Reveal High Levels of Free Zn^{2+}. *ACS Chem. Biol.* **2014**, *9*, 2111−2120.
(26) Hessels, A. M.; Chabosseau, P.; Bakker, M. H.; Engelen, W.; Rutter, G. A.; Taylor, K. M.; Merkx, M. EZinCh-2: A Versatile, Genetically Encoded FRET Sensor for Cytosolic and Intraorganelle Zn^{2+} Imaging. *ACS Chem. Biol.* **2015**, *10*, 2126−2134.
(27) Park, J. G.; Palmer, A. E. Quantitative Measurement of Ca^{2+} and Zn^{2+} in Mammalian Cells Using Genetically Encoded Fluorescent Biosensors. *Methods Mol. Biol.* **2014**, *1071*, 29−47.
(28) Carter, K. P.; Carpenter, M. C.; Fiedler, B.; Jimenez, R.; Palmer, A. E. Critical Comparison of FRET-Sensor Functionality in the Cytosol and Endoplasmic Reticulum and Implications for Quantification of Ions. *Anal. Chem.* **2017**, *89*, 9601−9608.
(29) Qin, Y.; Dittmer, P. J.; Park, J. G.; Jansen, K. B.; Palmer, A. E. Measuring Steady-State and Dynamic Endoplasmic Reticulum and Golgi Zn^{2+} with Genetically Encoded Sensors. *Proc. Natl. Acad. Sci. U. S. A.* **2011**, *108*, 7351−7356.
(30) Park, J. G.; Qin, Y.; Galati, D. F.; Palmer, A. E. New Sensors for Quantitative Measurement of Mitochondrial Zn^{2+}. *ACS Chem. Biol.* **2012**, *7*, 1636−1640.
(31) Kowada, T.; Watanabe, T.; Amagai, Y.; Liu, R.; Yamada, M.; Takahashi, H.; Matsui, T.; Inaba, K.; Mizukami, S. Quantitative Imaging of Labile Zn^{2+} in the Golgi Apparatus Using a Localizable Small-Molecule Fluorescent Probe. *Cell Chem. Biol.* **2020**, *27*, 1521−1531.
(32) Los, G. V.; Encell, L. P.; McDougall, M. G.; Hartzell, D. D.; Karassina, N.; Zimprich, C.; Wood, M. G.; Learish, R.; Ohana, R. F.; Urh, M.; Simpson, D.; Mendez, J.; Zimmerman, K.; Otto, P.; Vidugiris, G.; Zhu, J.; Darzins, A.; Klaubert, D. H.; Bulleit, R. F.; Wood, K. V. HaloTag: A Novel Protein Labeling Technology for Cell Imaging and Protein Analysis. *ACS Chem. Biol.* **2008**, *3*, 373−382.
(33) Kowada, T.; Watanabe, T.; Liu, R.; Mizukami, S. Protocol for Synthesis and Use of a Turn-on Fluorescent Probe for Quantifying Labile Zn^{2+} in the Golgi Apparatus in Live Cells. *STAR Protoc.* **2021**, *2*, 100395.
(34) Li, D.; Liu, L.; Li, W. H. Genetic Targeting of a Small Fluorescent Zinc Indicator to Cell Surface for Monitoring Zinc Secretion. *ACS Chem. Biol.* **2015**, *10*, 1054−1063.
(35) Li, D.; Chen, S.; Bellomo, E. A.; Tarasov, A. I.; Kaut, C.; Rutter, G. A.; Li, W. H. Imaging Dynamic Insulin Release Using a Fluorescent Zinc Indicator for Monitoring Induced Exocytotic Release (ZIMIR). *Proc. Natl. Acad. Sci. U. S. A.* **2011**, *108*, 21063−21068.
(36) Bagur, R.; Hajnóczky, G. Intracellular Ca^{2+} Sensing: Its Role in Calcium Homeostasis and Signaling. *Mol. Cell* **2017**, *66*, 780−788.
(37) Romani, A. M. P. Intracellular Magnesium Homeostasis. *Magnes. Cent. Nerv. Syst.* **2012**, *512*, 13−58.
(38) Ince, C.; Thio, B.; van Duijn, B.; van Dissel, J. T.; Ypey, D. L.; Leijh, P. C. J. Intracellular K^+, Na^+ and Cl^- Concentrations and Membrane Potential in Human Moncytes. *Biochim. Biophys. Acta* **1987**, *905*, 195−204.
(39) Grabowski, Z. R.; Rotkiewicz, K.; Rettig, W. Structural Changes Accompanying Intramolecular Electron Transfer: Focus on Twisted Intramolecular Charge-Transfer States and Structures. *Chem. Rev.* **2003**, *103*, 3899−4031.
(40) Szakács, Z.; Rousseva, S.; Bojtár, M.; Hessz, D.; Bitter, I.; Kállay, M.; Hilbers, M.; Zhang, H.; Kubinyi, M. Experimental Evidence of TICT State in 4-Piperidinyl-1,8-Naphthalimide-a Kinetic and Mechanistic Study. *Phys. Chem. Chem. Phys.* **2018**, *20*, 10155−10164.
(41) Kawabata, E.; Kikuchi, K.; Urano, Y.; Kojima, H.; Odani, A.; Nagano, T. Design and Synthesis of Zinc-Selective Chelators for Extracellular Applications. *J. Am. Chem. Soc.* **2005**, *127*, 818−819.
(42) Mataga, N.; Kaifu, Y.; Koizumi, M. Solvent Effects upon Fluorescence Spectra and the Dipolemoments of Excited Molecules. *Bull. Chem. Soc. Jpn.* **1956**, *29*, 465−470.
(43) Barik, A.; Kumbhakar, M.; Nath, S.; Pal, H. Evidence for the TICT Mediated Nonradiative Deexcitation Process for the Excited

https://doi.org/10.1021/acssensors.1c02153
ACS Sens. 2022, 7, 748−757

Coumarin-1 Dye in High Polarity Protic Solvents. *Chem. Phys.* **2005**, *315*, 277−285.
(44) Maret, W. Analyzing Free Zinc(II) Ion Concentrations in Cell Biology with Fluorescent Chelating Molecules. *Metallomics* **2015**, *7*, 202−211.
(45) Hessels, A. M.; Merkx, M. Genetically-Encoded FRET-Based Sensors for Monitoring Zn^{2+} in Living Cells. *Metallomics* **2015**, *7*, 258−266.
(46) Huang, Z.; Zhang, X. A.; Bosch, M.; Smith, S. J.; Lippard, S. J. Tris(2-Pyridylmethyl)Amine (TPA) as a Membrane-Permeable Chelator for Interception of Biological Mobile Zinc. *Metallomics* **2013**, *5*, 648−655.
(47) Gibson, W. T.; Chamberlain, M.; Parsons, J. F.; Brunskill, J. E.; Lock, S.; Safford, R. J. The effect and mode of action of zinc pyrithione on cell growth. I. in vitro studies. *Food Chem. Toxicol.* **1985**, *23*, 93−102.
(48) Carraway, R. E.; Dobner, P. R. Zinc pyrithione induces ERK- and PKC-dependent necrosis distinct from TPEN-induced apoptosis in prostate cancer cells. *Biochim. Biophys. Acta* **2012**, *1823*, 544−557.
(49) Rudolf, E.; Červinka, M. Zinc pyrithione induces cellular stress signaling and apoptosis in Hep-2 cervical tumor cells: the role of mitochondria and lysosomes. *Biometals* **2010**, *23*, 339−354.
(50) Morgan, M. T.; Bourassa, D.; Harankhedkar, S.; McCallum, A. M.; Zlatic, S. A.; Calvo, J. S.; Meloni, G.; Faundez, V.; Fahrni, C. J. Ratiometric Two-Photon Microscopy Reveals Attomolar Copper Buffering in Normal and Menkes Mutant Cells. *Proc. Natl. Acad. Sci. U. S. A.* **2019**, *116*, 12167−12172.
(51) Watanabe, S.; Amagai, Y.; Sannino, S.; Tempio, T.; Anelli, T.; Harayama, M.; Masui, S.; Sorrentino, I.; Yamada, M.; Sitia, R.; Inaba, K. Zinc Regulates ERp44-Dependent Protein Quality Control in the Early Secretory Pathway. *Nat. Commun.* **2019**, *10*, 603−619.

https://doi.org/10.1021/acssensors.1c02153
ACS Sens. 2022, 7, 748−757